Dynamic equivalent of a real distribution grid hosting photovoltaic and synchronous generators

Gilles Chaspierre[1,*], Mehdi Ghazavi Dozein[2], Guillaume Denis[3], Patrick Panciatici[3] and T. Van Cutsem[1, 4]

[1]Dept. of Electrical Engineering and Computer Science, University of Liège, Belgium

[2]School of Electrical and Electronic Eng., The University of Melbourne

[3]Research & Development Dept., RTE, Paris La Défense, France

[4]Fund for Scientific Research (FNRS), Belgium

Abstract

This paper presents a methodology to derive a reduced-order, "grey-box" model of an active distribution network. This dynamic equivalent is intended for dynamic simulations of large disturbances taking place in the transmission system. To deal with the uncertainty affecting dynamic model parameters, Monte-Carlo simulations are used, and the parameters of the equivalent are adjusted to match as close as possible the average randomized system responses. To avoid over-fitting, multiple disturbances are considered; they are automatically selected among a set of candidates. Moreover, to reduce the computational burden, only parameters with significant impact are adjusted in the identification procedure. Simulation results are reported on a real Australian distribution grid. The latter hosts synchronous generators and residential photovoltaic units. Its loads are modelled with a static and a motor part.

Index Terms: Active distribution network, inverter-based and synchronous generators, dynamic equivalent, grey-box model, Monte-Carlo simulations

*** Corresponding author. E-mail: g.chaspierre@uliege.be**

1. Introduction

Environmental concerns drive the sustained replacement of conventional generation units by Inverter-Based Generators (IBGs) such as PhotoVoltaic (PV) units or wind turbines. An important part of these IBGs is connected to lower voltage levels, which increases the complexity of distribution systems, and the resulting Active Distribution Networks (ADNs) will have a growing influence on the whole power system dynamics [1]. This problem arises particularly in Australia where the total distributed PV capacity has significantly increased in the past few years and is expected to keep growing in the future, progressively replacing conventional generation units with Synchronous Generators (SGs) connected at transmission level [2]. This replacement induces a reduction of the short-circuit level in the transmission grid, which can result in severe voltage sensitivity, and exacerbates the influence of ADNs on power system dynamics following contingencies [3]. As an illustration, Fig. 1 shows the forecast of combined PV and battery installed capacity in the Australian national electricity market [4]. It is expected to increase to between 12 and 21 GW of capacity by 2030.

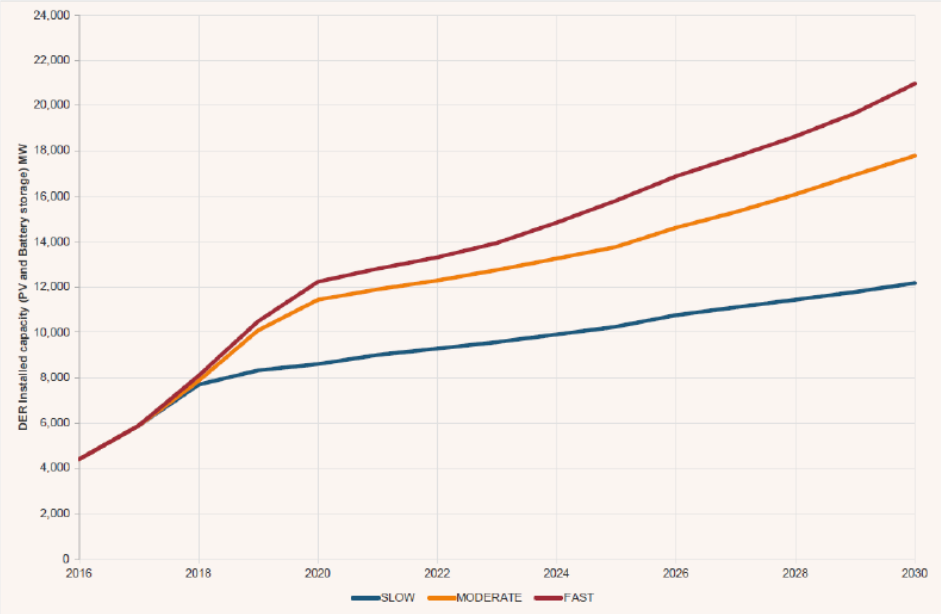

Figure 1 Forecast of combined PV and battery installed capacity across the Australian electricity market

Therefore, it becomes urgent for the Australian Energy Market Operator (AEMO), responsible for power system security, to account for the contribution of ADNs in their dynamic simulation studies. However, owing to the huge complexity of maintaining a combined transmission and distribution system model, it makes more sense for AEMO to use reduced-order models (or dynamic equivalents) that offer a good compromise between simplicity and accuracy. The parameters of those equivalents are tuned to match as closely as possible the unreduced ADN dynamic responses to disturbances. The latter response could be obtained either from measurements or by simulation. Considering that the focus of this work is on relatively rare, large-disturbance events (such as faults in the transmission grid), recorded measurements are not (or almost not) available, and a simulation-based approach is necessary. Hence, the first step consists in setting up a reference model for the original (unreduced) ADN.

While it can be assumed that the network model is sufficiently accurate, dynamic models, on the other hand, are affected by uncertainty. For instance, parameters of motors are usually set to "typical" values (such as those that can be found in [5] and related references) to account for a population of small motor loads. Regarding IBGs, grid codes allow for a range of permissible behaviours [6], [7]. To deal with such uncertainties, a traditional approach is to resort to Monte-Carlo (MC) simulations [8]. For a given

disturbance, dynamic responses are generated for randomized variations of the uncertain parameters [9]. Averages and standard deviations of the time responses provide useful information on the time-varying impact of parameter uncertainty.

Deriving the dynamic equivalent is the second step. A reduced model of the "grey-box" type has been considered, as defined and recommended in [10] and [11], for instance. It is intended to be attached to the transmission system model. The parameters of the equivalent are obtained by weighted least-square minimization, where the weights reflect the dispersion of the randomized dynamic responses. It should correctly reproduce the ADN response to large disturbances taking place in the transmission system. The latter is not modelled. Only the impact of faults on the voltage at the connection point with the ADN is considered. Multiple disturbances are used in order for the equivalent to not overfit one of them. Some disturbances cause partial disconnection of the ADN-connected IBGs. To avoid handling too many contingencies, they are processed recursively so as to select the smallest possible subset from an initial set of candidate disturbances, from which parameters of the equivalent model are adjusted. Finally, to make the reduced model more consistent and interpretable, a procedure is used to discard from the identification parameters with non-significant impact on the performance of the equivalent.

Some of the methods reported in this paper have been described in previous publications by the authors (e.g. [9, 12]). The main novelty, however, lies in the simulation results, which have been obtained on a new, real and more complex ADN. One of its features is the presence of SGs, whose dynamic responses are significantly different from those of IBGs. It is noteworthy that the simulations have considered a plausible future scenario with Australian distributed PV units obeying an updated grid code similar to IEEE std 1547-2018, as suggested in [4], with retro-fitting of existing units. This illustrates the ability of the proposed grey-box equivalent model to follow changes in the grid code requirements.

The rest of the paper is organized as follows. The models of the unreduced ADN and its equivalent are presented in Sections 2 and 3, respectively. Section 4 deals with the optimization of the equivalent parameters. Simulation results are reported in Section 5, while conclusions are offered in Section 6.

2. Unreduced ADN modelling

The ADN model aims at rendering the impact on transmission system dynamics of numerous loads and generators dispersed in a distribution grid. Rotor angle, frequency and voltage stability studies are targeted. The focus is on transients lasting up to 10 to 20 seconds after a large disturbance.

2.1. Network

The model of the Australian 22-kV distribution grid includes 92 buses. It is connected to the 63-kV sub-transmission network through a single transformer. Its one-line diagram is given in Fig. 2. The grid hosts numerous small-scale dispersed PV units for a total capacity of 5.3 MW as well as eight SGs all connected to the same bus and accounting for a co-generation power plant. All SGs have the same technical characteristics, in particular a nominal apparent power of 1.5 MVA. Therefore, a single SG is considered in the model, whose capacity is scaled to the number of individual SGs in operation.

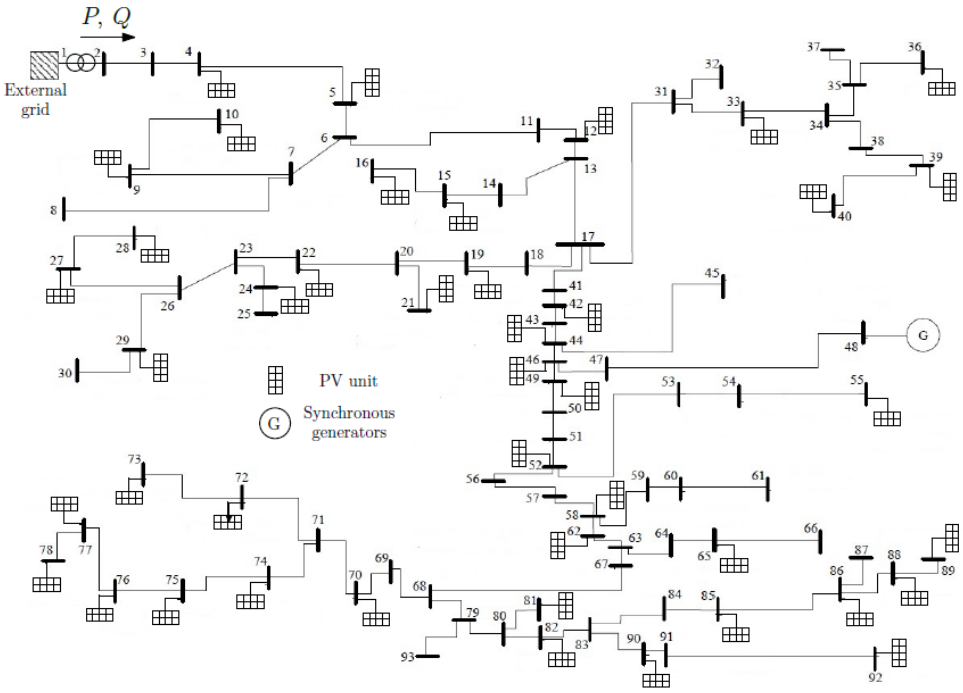

Figure 2 One-line diagram of the ADN

2.2. Load model

The generic load model considered is depicted in Fig. 3. It is split into a standard exponential model and a third-order Induction Motor (IM) model. Initially, the motor consumes a fraction m of the total active power and the compensation capacitor is adjusted to satisfy a specified power factor $\cos\phi_m$. The well-known equivalent circuit of the IM with its parameters is given in Fig. 4, in which the electrical part is "static" and the rotor angular speed ω_r varies according to the rotor motion equation:

$$2H_{mot}\frac{d}{dt}\omega_r = T_e - T_{mo}(A\omega_r^2 + B\omega_r + C), \quad (1)$$

where H_{mot} is the inertia constant, A (resp. B) is the fraction of the mechanical torque varying quadratically (resp. linearly) with ω_r, and $A + B + C = 1$.

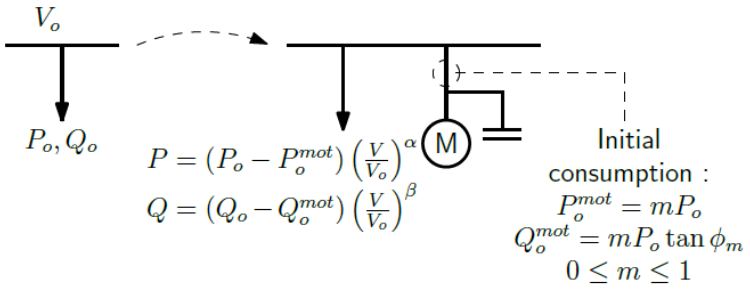

Figure 3 Load model decomposed into exponential and motor parts

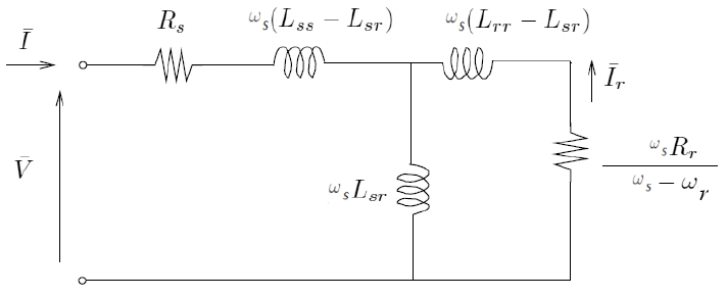

Figure 4 Equivalent circuit of the IM

2.3. IBG model

A generic model of IBG is used for each PV unit. It captures the variations of injected current with respect to the terminal voltage. The latter is shown in block-diagram form in Fig. 5. It involves time constants on the voltage measurement and on the current control loops. The embedded controls meet recent grid-code requirements (e.g. [6], [7]), such as Low Voltage Ride-Through (LVRT) and reactive current injection for voltage support. The LVRT curve implemented is defined by six parameters, as shown in Fig. 6.(a). For voltage support, the reactive current i_Q is a piecewise linear function of the measured voltage, as shown in Fig. 6.(b), where V_m is the measured terminal voltage, i_{Q0} the pre-disturbance reactive current and I_{nom} the IBG nominal current.

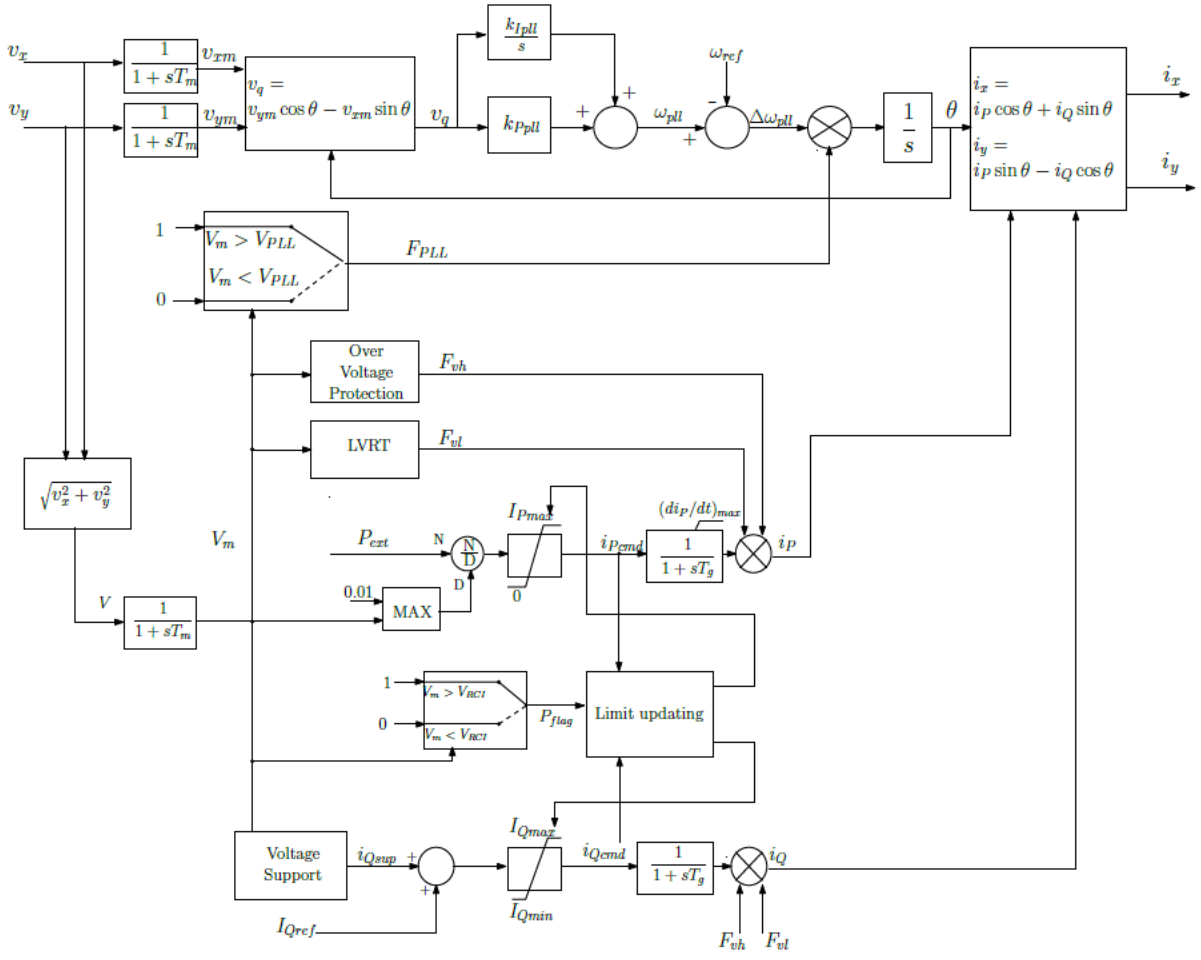

Figure 5 Block diagram of the IBG model

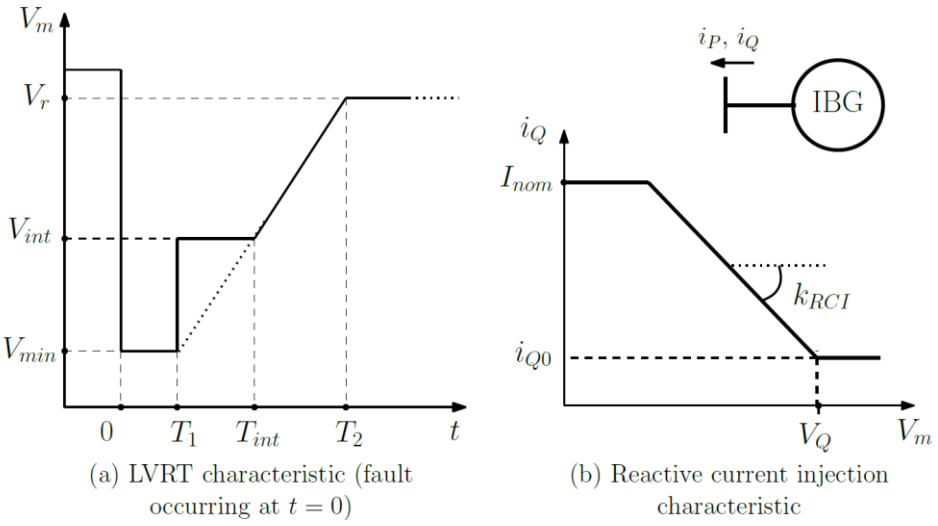

(a) LVRT characteristic (fault occurring at $t = 0$)

(b) Reactive current injection characteristic

Figure 6 IBG: controls responding to voltage deviation

In low voltage conditions ($V_m < V_Q$ in Fig. 6.(a)), priority is given to the reactive current injection which may lead to curtailing the active current, in order to not exceed the nominal current of the converter. Once the voltage returns to normal values, the IBG active current recovers its pre-disturbance value, but with an upper limit on its rate of recovery. This rate has been chosen in the range given in [13].

Finally, the IBG phase-locked loop is taken into account, though with a generic model, since it introduces a delay that may affect the overall dynamic response of the IBG.

Additional details on the model can be found in [14].

2.4. Synchronous generator model

The SGs connected at distribution level are represented with a fifth-order model of the synchronous machine [15], a constant mechanical power and a generic model of the excitation system including a reactive power control loop and a simple exciter, as shown in Fig. 7. The model is inspired from "Var controller Type II" model in [16], p.38, which is representative of excitation systems for small synchronous machines connected at distribution level that are not supposed to regulate the system voltage.

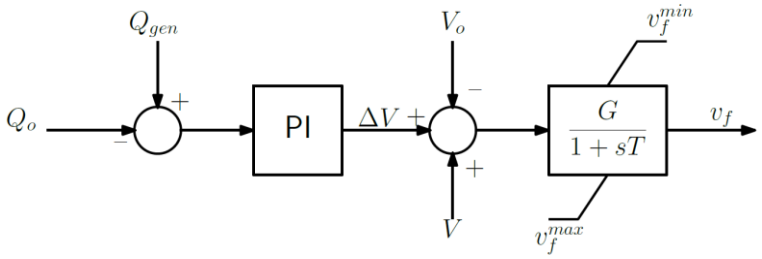

Figure 7 SG excitation system : Q_{gen} is the reactive power produced, V the terminal voltage and v_f the field voltage [16]

2.5. Dealing with model uncertainties

It is assumed that the dynamic models of loads and IBGs are qualitatively correct but involve uncertain parameters. On the other hand, due to their size, location and monitoring, the SGs are considered to have accurately known models and parameters.

As mentioned in the Introduction, MC simulations are used to assess the impact of this uncertainty on the dynamic response of the unreduced system. The uncertain parameters are randomized from one MC simulation to another but also from one load and one IBG to another. For the above-mentioned reason, the SG model is not randomized in the MC simulations.

Let s be the number of randomly drawn instances of model parameters, gathered in a vector $\boldsymbol{p}$. The variables of interest are the active power P and reactive power Q entering the ADN. For the j-th disturbance ($j = 1, \dots, d$), the i-th instance $\boldsymbol{p}_i$ of $\boldsymbol{p}$ ($i = 1, \dots, s$) and a discrete instant k, the following values are extracted from the MC simulations:

$P(j, k, \boldsymbol{p}_i)$ the active power at time k obtained with $\boldsymbol{p}_i$

$Q(j, k, \boldsymbol{p}_i)$ the corresponding reactive power

$\mu_P(j, k)$ the average of the s values of $P(j, k, \boldsymbol{p}_i)$

$\mu_Q(j, k)$ the average of the s values of $Q(j, k, \boldsymbol{p}_i)$

$\sigma_P(j, k)$ the standard deviation of the s values of $P(j, k, \boldsymbol{p}_i)$

$\sigma_Q(j, k)$ the standard deviation of the s values of $Q(j, k, \boldsymbol{p}_i)$

3. Dynamic equivalent model

3.1. Topology of the equivalent

The topology of the equivalent is shown in Fig. 8. The connection to the transmission grid is through a single transformer, which is retained in the equivalent. The dispersed loads, the dispersed IBGs and the SGs of the unreduced system are aggregated into respectively a single load, a single IBG and a single SG, behind equivalent impedances $R_a + jX_a$, $R_b + jX_b$ and $R_c + jX_c$, accounting for network effects. A configuration such as that of Fig. 8 is recommended in [17] as it can differentiate generators by technical characteristics and/or grid requirements.

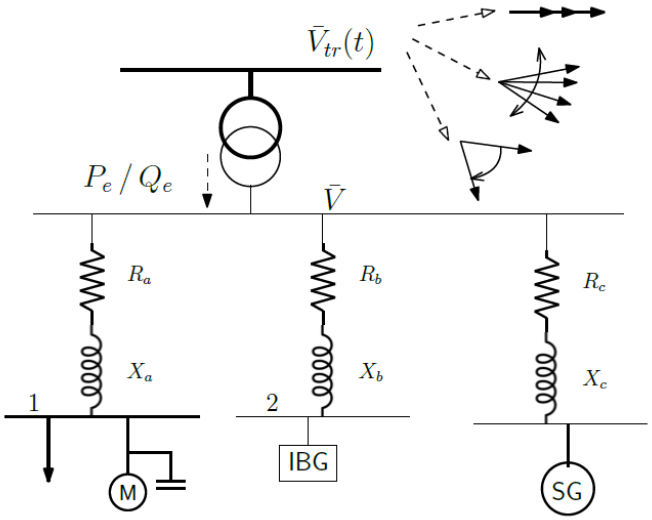

Figure 8 Topology of the equivalent

3.2. Models in the equivalent

The model used for the aggregated load in the equivalent is the same as that used for individual loads in the unreduced system (see Section 2.2). The same applies to the equivalent SG (see Section 2.4).

The model used for the aggregated IBG includes the features of the model used for individual IBGs in the unreduced system (see Section 2.3). However, since the disconnection of IBGs under low voltage conditions can have a tremendous impact on the ADN response and, to some extent, on the whole power

system stability, the aggregated IBG must account for the tripping of some individual IBGs in the original system. Therefore, instead of following a LVRT characteristic, the aforementioned situation is accounted by providing the aggregated IBG with a "partial tripping" feature, as shown in Fig. 9. The variable l represents the fraction of IBGs still connected. When the voltage V of the equivalent IBG falls below the V_{pt} threshold, l drops to γ, which corresponds to loosing a fraction $1-\gamma$ of the IBGs. For further voltage drops, l decreases linearly with V. Full disconnection ($l=0$) takes place for $V=V_{ft}$. As illustrated in Fig. 9, when V recovers, l remains at the l_{min} value corresponding to the voltage nadir. The technique is a simplified version of the one considered in [14] and similar to the one used in [18].

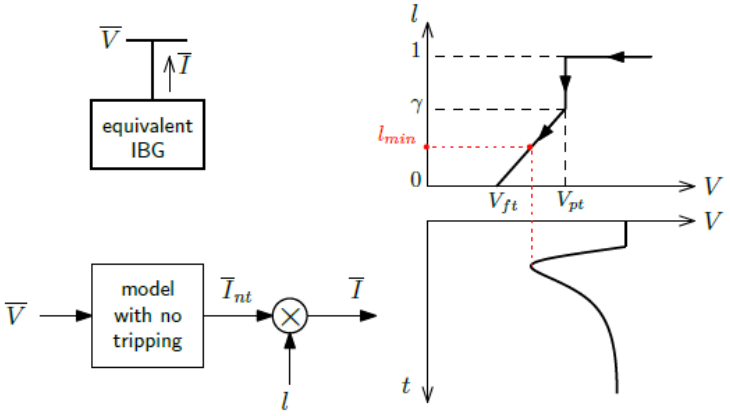

Figure 9 "Partial tripping" feature of the aggregated IBG

4. Identification of the ADN equivalent

To avoid over-fitting a particular scenario, a number d of training disturbances are considered. Each of them consists of imposing large variations of the amplitude, the phase angle, or the frequency of the voltage source $\bar{V}_{tr}$ replacing the transmission system (see Fig. 8). The accuracy of the equivalent is assessed on its active power P_e and reactive power Q_e.

4.1. Weighted least-square identification

The parameters to identify are grouped in a vector $\boldsymbol{\theta}$. The latter is adjusted so that, for each discrete time k and for all disturbances j, the active power $P_e(\boldsymbol{\theta},j,k)$ (resp. the reactive power $Q_e(\boldsymbol{\theta},j,k)$) of the equivalent model approaches in the least square sense the average $\mu_P(j,k)$ (resp. $\mu_Q(j,k)$) defined in Section 2.5.

Thus the following constrained optimization is considered:

$$\boldsymbol{min}_{\boldsymbol{\theta}}\ F(\boldsymbol{\theta}) = \frac{1}{d}\sum_{j=1}^{d}\left[F_P(\boldsymbol{\theta},j) + F_Q(\boldsymbol{\theta},j)\right] \tag{2}$$

with

$$F_P(\boldsymbol{\theta},j) = \frac{1}{N}\sum_{k=1}^{N}\left[\frac{P_e(\boldsymbol{\theta},j,k) - \mu_P(j,k)}{\sigma_P(j,k)}\right]^2 \tag{3}$$

$$F_Q(\boldsymbol{\theta},j) = \frac{1}{N}\sum_{k=1}^{N}\left[\frac{Q_e(\boldsymbol{\theta},j,k) - \mu_Q(j,k)}{\sigma_Q(j,k)}\right]^2 \tag{4}$$

$$\boldsymbol{\theta}^L \leq\ \boldsymbol{\theta} \leq \boldsymbol{\theta}^U \tag{5}$$

where N is the number of discrete times of the simulation. The bounds $\boldsymbol{\theta}^L$ and $\boldsymbol{\theta}^U$keep $\boldsymbol{\theta}$ in feasible range of values.

Note that each term in (3) (resp. (4)) is weighted by the inverse of the variance $\sigma_P^2(j,k)$ (resp. $\sigma_Q^2(j,k)$) to reflect the dispersion of MC responses. The rationale is to allow a larger deviation from the average when the randomized responses are more widely dispersed, i.e. more uncertain.

4.2. Solving the optimization problem

Standard mathematical programming methods can hardly be envisaged to solve the least-square minimization problem (2)-(5). Instead, an Evolutionary Algorithm (EA), namely Differential Evolution (DE) [19], has been selected, after testing quite a number of the existing meta-heuristic methods. A systematic comparison with other algorithms is outside the scope of this research. While another method could offer a most welcome speed-up, DE has been found a reliable solver for the optimization problem (2)-(5) in a very large number of cases. More information can be found in [14], in particular regarding the proper tuning of the algorithm key parameters (e.g., the crossover and mutation factors).

4.3. Selection of training disturbances

When the number of disturbances d increases, the risk of over-fitting one of them decreases. On the other hand, increasing the number of disturbances can substantially increase the computational burden of the minimization (2)-(5). To tackle this problem, a subset of the candidate disturbances is automatically selected, from which the parameters are identified. The idea is to progressively add training disturbances until the equivalent is found sufficiently accurate with respect to all the other, non-trained disturbances. After a new disturbance is involved in the identification, $\boldsymbol{\theta}$ is adjusted such that the equivalent is sufficiently accurate for all training scenarios. For a given estimate $\widehat{\boldsymbol{\theta}}$, the newly added disturbance is the one for which the currently identified equivalent shows the worst accuracy.

4.4. Discarding "non-significant" parameters

For a better interpretability and consistency of the model, a procedure is used to discard the less significant parameters of the least-square minimization. It consists of adding a penalty term to (2) :

$$\boldsymbol{min}_{\boldsymbol{\theta}}\ F(\boldsymbol{\theta}) + \lambda\sum_{l=1}^{n}\left|\theta_l^{ref} - \theta_l\right| \tag{6}$$

where λ is a scaling factor, n is the size of $\boldsymbol{\theta}$ and $\boldsymbol{\theta}^{ref}$ is a reference value for the parameters. The penalty term tends to make θ_l departs from θ_l^{ref} only if it yields a significant decrease of $F(\boldsymbol{\theta})$, i.e. if θ_l has a significant influence on $F(\boldsymbol{\theta})$, thereby making the dynamic response of the equivalent more accurate.

The procedure starts with a large value of λ, which yields $\widehat{\boldsymbol{\theta}} \cong \boldsymbol{\theta}^{ref}$. Then, λ is decreased steps by steps and, for each value the minimization problem (2)-(5) is solved with the penalty term as in (6). This is repeated until $F(\widehat{\boldsymbol{\theta}})$ falls below a tolerance. At this point, the components of $\widehat{\boldsymbol{\theta}}$ and $\boldsymbol{\theta}^{ref}$ are compared. If, for the l-th component ($l = 1, \dots, n$) :

$$\frac{\left|\hat{\theta}_l - \theta_l^{ref}\right|}{\theta_l^{ref}} \leq \delta \tag{7}$$

the parameter of concern is considered to have little impact and is removed from the least-square minimization problem.

$\boldsymbol{\theta}^{ref}$ is set to the middle of the interval in which the parameters of the equivalent vary (see (5)), i.e.

$$\boldsymbol{\theta}^{ref} = \frac{\boldsymbol{\theta}^L + \boldsymbol{\theta}^U}{2} . \tag{8}$$

While it is rather easy to choose such intervals for the dynamic model parameters (of the load, the IBG, and the SG), it is less the case for the equivalent network impedances $R_a + jX_a$, $R_b + jX_b$ and $R_c + jX_c$ (see Fig. 8). Instead, a network reduction technique has been used to obtain the $\boldsymbol{\theta}^{ref}$ value of those impedances. The procedure is detailed in the Appendix.

5. Simulation results

5.1. Operating point and disturbances

The system, presented in Section 2.1, has the following initial operating point. A single SG is in operation and produces 1 MW / 0.15 Mvar. The PV units operate at 50 % of their capacity, with unity power factor. The distribution grid feeds a total load of 18.2 MW. It receives a net power of 14.8 MW / 3.2 Mvar from the upper voltage level.

Only voltage dip disturbances are considered for the identification. The candidate disturbances are listed in Fig. 10 and are characterized by a depth ΔV, which reflects the fault location in the transmission system and a duration ΔT typical of fault clearing by (main or back-up) protections. They are applied to the s instances of the unreduced system and to the equivalent when optimizing its parameters $\boldsymbol{\theta}$.

The dynamic evolutions of the active power P and reactive power Q entering the ADN are collected over four seconds. The RAMSES software for dynamic simulation in phasor mode has been used [20]; the average time step size is 0.005 s.

disturb. No	ΔV (pu)	ΔT (s)
1	0.2	0.10
2	0.2	0.25
3	0.3	0.10
4	0.3	0.25
5	0.4	0.10
6	0.4	0.25
7	0.5	0.10
8	0.5	0.25
9	0.6	0.10
10	0.6	0.25
11	0.7	0.10
12	0.7	0.25
13	0.8	0.1
14	0.8	0.25

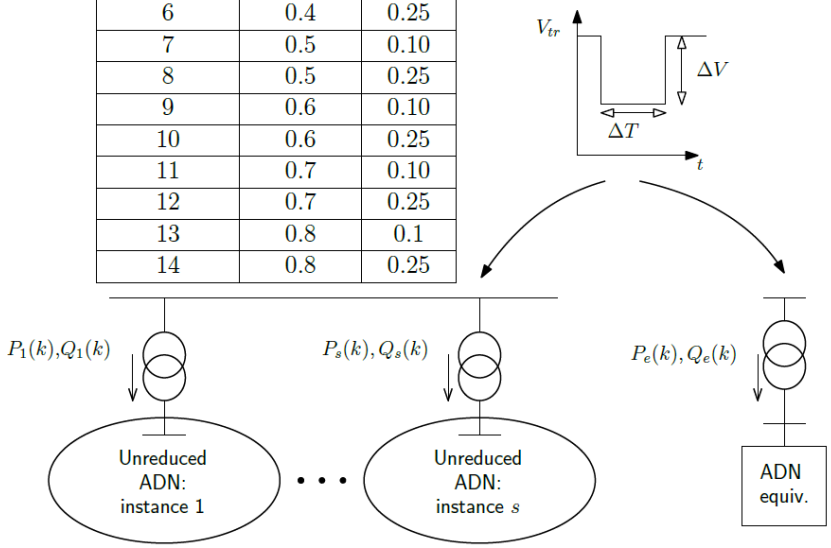

Figure 10 The 14 candidate disturbances used in MC simulations and in the equivalent identification

5.2. Monte-Carlo simulations

The parameters randomized in the MC simulations and their corresponding range of values are shown in Table. 1. For the IMs, the range of parameter values has been chosen based on [5]. For the IBGs, the range of parameter values are selected according to permissible behaviour allowed by grid codes [6], [7]. As previously mentioned, the parameters of the synchronous machine are not randomized since it is assumed that its model is accurately known. The nominal currents of IBGs are also assumed to be known, and are not randomized either. Last but not least, the minimum voltage threshold V_{min} in the LVRT curve (see Fig. 6.(a)) has been also randomized. It is treated as a discrete random variable that can take the values 0 or 0.3 pu. In the former case, the IBG never disconnects from the grid. In the latter case, disconnections occur for severe voltage dips. This allows to take into account the uncertainty on IBGs tripping in response to a short-circuit.

Figures 11 and 12 show the randomized time evolutions of respectively P and Q in response to disturbance No. 4 (see table in Fig. 10). Powers take positive values when entering the ADN. All curves start from the same value, since the same operating point is considered, and come back to that value, since this rather mild disturbance does not trigger PV units disconnection.

Table 1 List of randomized parameters and associated range of values

Parameter	***Mathematical expression***	***Related figure or equation***	***Range of values***
Motor stator resistance	R_s	Fig. 4	[0.03 0.13] pu
Motor rotor resistance	R_r	Fig. 4	[0.03 0.13] pu
Motor magnetizing reactance	L_{sr}	Fig. 4	[1.8 3] pu
Motor stator leakage reactance *(L_{ss}: stator reactance)*	$L_{ss} - L_{sr}$	Fig. 4	[0.07 0.15] pu
Motor rotor leakage reactance *(L_{rr}: rotor reactance)*	$L_{rr} - L_{sr}$	Fig. 4	[0.06 0.15] pu
Inertia constant of the motor	H_{mot}	Eq. (1)	[0.26 1] s
Motor fraction of quadratic mechanical torque	A	Eq. (1)	[0.2 1]
Motor load factor *(S_{nom} : nominal apparent power)*	P_{mot0}/S_{nom}	-	[0.4 0.6]
Fraction of initial motor active power consumption	m	Fig. 3	[0.1 0.3]
Initial motor power factor	$cos\ \emptyset_m$	Fig. 3	[0.9 0.95]
Load static part exponent	α	Fig. 3	[1 2]
Load static part exponent	β	Fig. 3	[1.5 3]
IBG rate of active current recovery	$(di_p/dt)_{max}$	Fig. 5	[0.2 0.5] pu/s
IBG : PLL response time	τ_{PLL}	Fig. 5	[0.05 0.15] s
IBG : current controller time constant	T_g	Fig. 5	[0.02 0.03] s
IBG : slope of reactive current vs. voltage	k_{RCI}	Fig. 6.b	[2 6] pu/pu
IBG: voltage threshold of reactive injection	V_Q	Fig. 6.b	[0.85 0.95] pu
IBG : minimum voltage threshold of LVRT	V_{min}	Fig. 6.a	{0, 0.3} pu

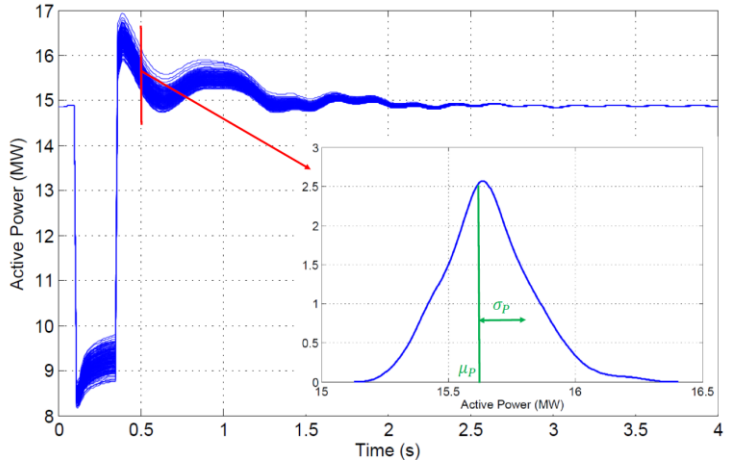

Figure 11 Randomized evolutions of P; disturbance No. 4

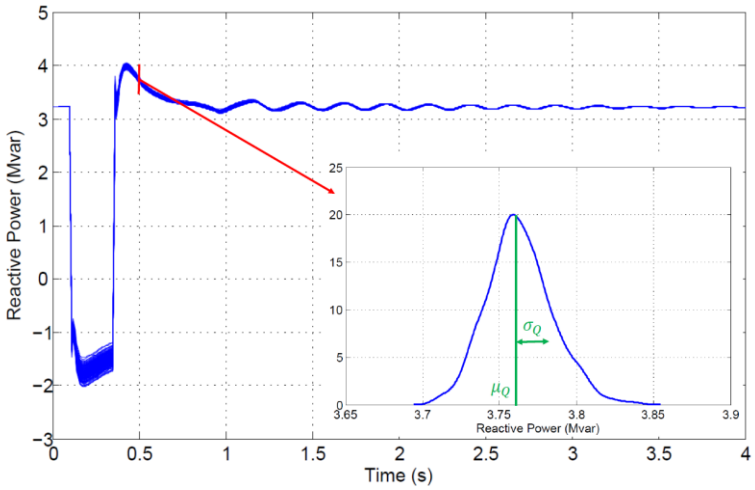

Figure 12 Randomized evolutions of Q; disturbance No. 4

The plots also show the distributions of power values at $t = 0.5$ s, as well as the corresponding μ_P, σ_P, μ_Q and σ_Q values. The small dispersion of reactive power evolutions is explained by the fact that they are mainly influenced by the SG response, whose parameters have not been randomized.

The overall evolution is explained as follows. During the voltage dip, the load with exponential model decreases while the PV units curtail their active current to leave room for reactive current injection. This, together with the additional reactive current injection from the SG, causes a reactive power flow reversal during the voltage dip, as confirmed by Fig. 12 where reactive powers temporarily take negative values. The small reactive power oscillation after voltage recovery originates from the AVR of the SG. When the voltage recovers to its initial value, so do the powers of loads with exponential model, while the motors draw some additional power, due to their re-acceleration. The slight active power oscillation after the voltage dip comes from the SG. Furthermore, after voltage recovery, the PV units ramp up their active power. This takes between one and two seconds; the effect can be seen in Fig. 11.

5.3. Identification of the equivalent

In addition to the parameters listed in Table 1, the equivalent includes three resistances and three reactances (see Fig. 8) as well as three parameters accounting for the "partial tripping" (see Fig. 9). Although the corresponding parameters were not randomized in the MC simulations of the unreduced system, when dealing with the equivalent, the IBG nominal current I_{nom}, the SG nominal apparent power S_{nom}^{SG} and the SG inertia constant H_{SG} have been included in $\boldsymbol{\theta}$. Indeed, further simulations (not reported here) have shown that by slightly adjusting these three parameters, the accuracy of the

equivalent is significantly improved. All in all, 29 parameters are gathered in $\boldsymbol{\theta}$. The method outlined in Section 4.4 allows discarding 19 parameters, which are merely set to typical values. The retained and the discarded parameters are listed in Table 2, respectively.

Table 2 Retained and discarded parameters in the equivalent

Component	***Retained***	***Discarded***
Network	-	$R_a, R_b, R_c, X_a, X_b, X_c$
Load	$L_{ss} - L_{sr}$, H_{mot}	$R_s, R_r, L_{sr}, L_{rr} - L_{sr}, A, {}^{P_{moto}}/_{S_{nom}}$, $m, cos\ \emptyset_m, \alpha, \beta$
IBG	$I_{nom}, (di_p/dt)_{max}, k_{RCI}, \gamma, V_{pt}, V_{ft}$	τ_{PLL}, T_g, V_Q
SG	S_{nom}^{SG}, H_{SG}	-

It can be seen that I_{nom}, S_{nom}^{SG} and H_{SG} are retained as significant by the procedure of Section 4.4, which confirms that these parameters play an important role in the accuracy of the equivalent. On the other hand, neither the resistances R_a, R_b, R_c nor the reactances X_a, X_b, X_c are retained, which tends to confirm that the impedances estimated by network reduction (see Appendix) are accurate enough. It is recalled that those values are used in $\boldsymbol{\theta}^{ref}$.

The procedure of Section 4.3 is performed in two steps as described next.

In a first step, scenarios without PV unit disconnection, namely disturbances No. 1 to 12 (see table in Fig. 10) are considered. The λ, V_{pt} and V_{ft} parameters are left aside and the least square minimization is applied to a $\boldsymbol{\theta}$ vector including the remaining seven parameters. The procedure outlined in Section 4.3 selects five of the twelve disturbances, namely No 4, 5, 6, 7 and 12, in the training set.

In a second step, the identification focuses on the γ, V_{pt} and V_{ft} parameters. The previously seven parameters are fixed to the values determined in the first step. The whole set of 14 disturbances is now considered, thus including disturbances No 13 and 14, which trigger PV units disconnection. The procedure of Section 4.3 adds disturbance No 13 to the training set.

5.4. Accuracy of the equivalent

For illustration purposes, the accuracy of the equivalent is shown in response to disturbance No 14, for which some PV units disconnect. Note that this disturbance was not selected to enter the training set.

Figure 13 shows with dotted line the evolution of the active power P_e in the equivalent, for the intermediate $\widehat{\boldsymbol{\theta}}$ obtained after the first step. As γ, V_{pt} and V_{ft} have not yet been optimized, the tripping of PV units is ignored and the response is inaccurate. The corresponding response for the final $\widehat{\boldsymbol{\theta}}$ obtained after the second step is shown with solid black line. It matches perfectly the average response μ_P, targeted by the least-square minimization, shown with red line. In particular both curves end up in the same value, demonstrating the ability of the equivalent to estimate the amount of disconnected PV units, even for a disturbance not involved in its training.

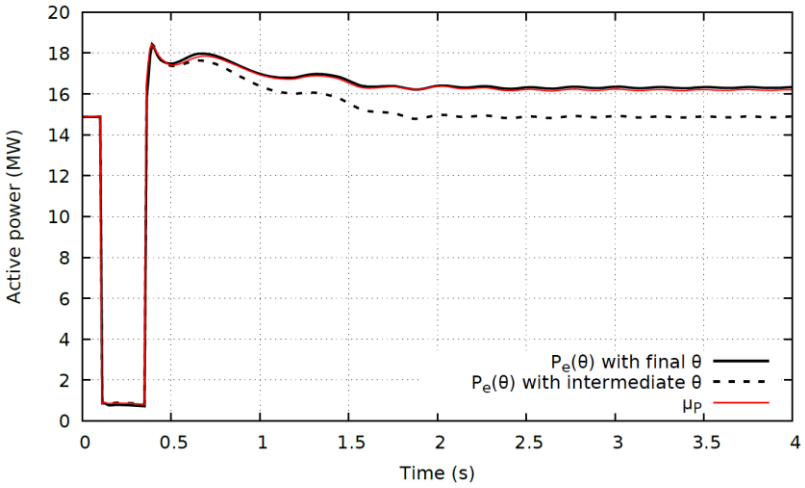

Figure 13 Active power responses to the non-trained disturbance No 14

Similar curves relative to the reactive power Q_e in the equivalent are given in Fig. 14. They confirm the accuracy of the equivalent for the reactive part.

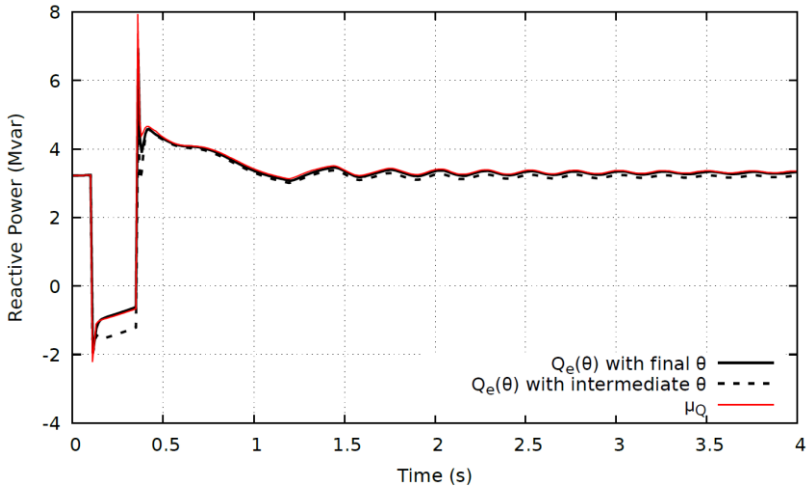

Figure 14 Reactive power responses to the non-trained disturbance No 14

5.5. Validation of the equivalent for another type of disturbance

Figures 15 and 16 show the active and reactive power responses of the equivalent to a very different, non-trained disturbance, namely an oscillation of the magnitude and phase angle of $\overline{V}_{tr}$ (see Fig. 8). This would render the effect of a rather severe electromechanical inter-area oscillation taking place in the transmission system. The imposed variation of the voltage magnitude V_{tr} and phase angle δ_{Vtr} are shown in Fig. 17.

The curves in red in Figs. 15 and 16 show the average evolutions μ_P and μ_Q, obtained from the randomized responses of the unreduced system to the disturbance of concern.

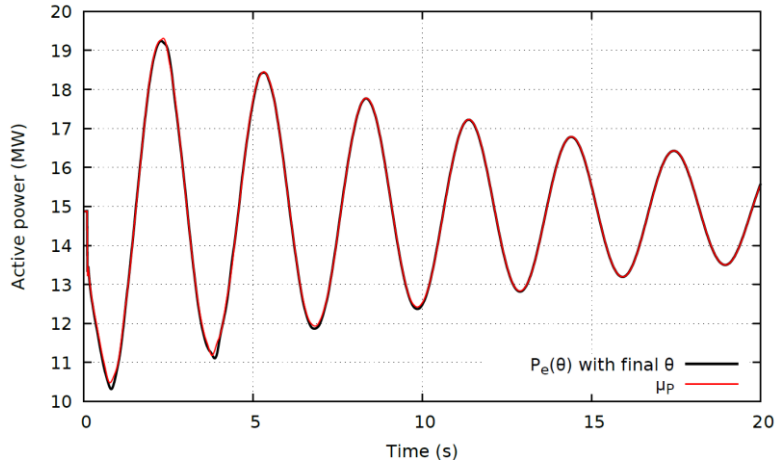

Figure 15 Active power responses to an electromechanical oscillation

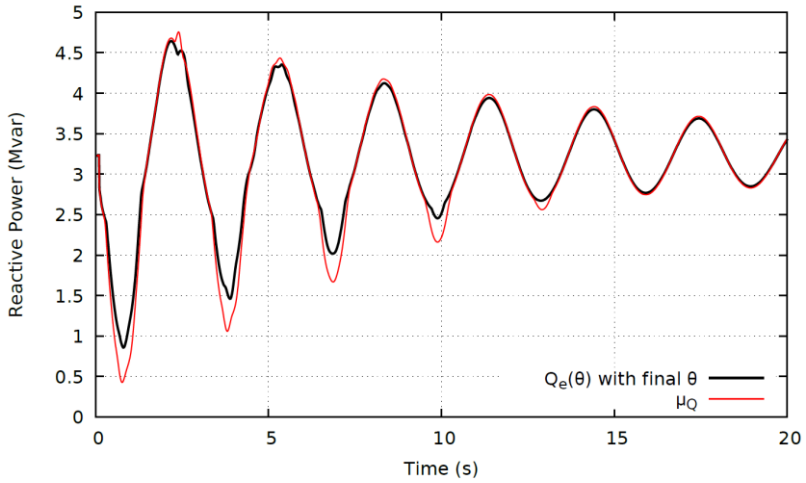

Figure 16 Reactive power responses to an electromechanical oscillation

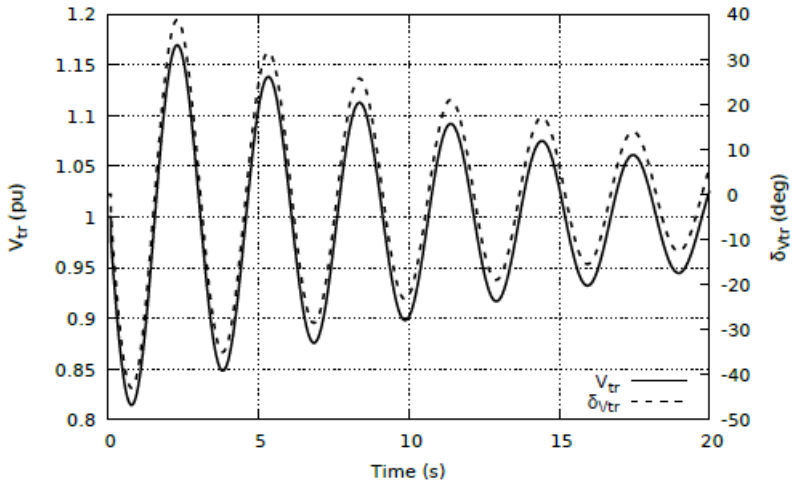

Figure 17 Voltage magnitude and phase angle oscillation

The active power response of the equivalent matches almost perfectly the reference evolution. As regards the reactive power, while the overall accuracy is also very good, some discrepancies are observed during the first four voltage nadirs. This is due to a small lack of reactive power production by the equivalent IBG, with respect to the PV units dispersed in the original system. As an illustration, the reactive power produced by the equivalent IBG is plotted in Fig. 18. The four "pulses" correspond to the four nadirs of the reactive power evolution in Fig. 16.

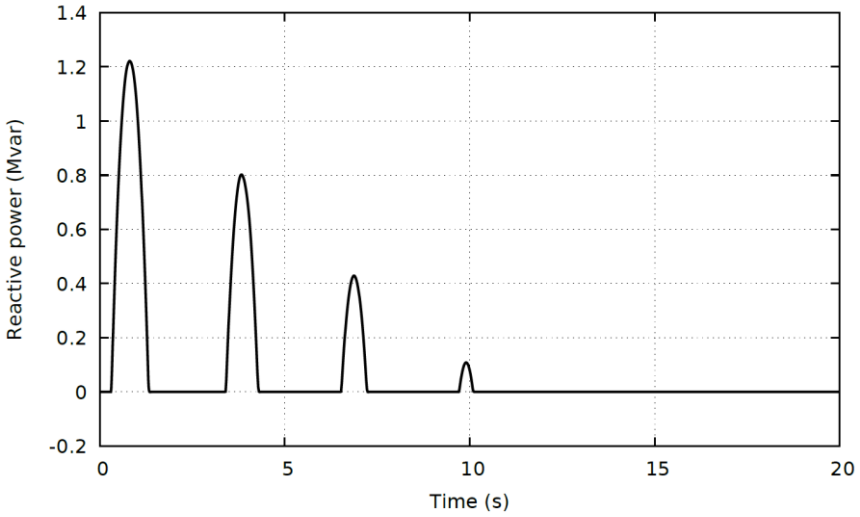

Figure 18 Reactive power produced by the equivalent IBG in response to an electromechanical oscillation

6. Conclusion

The fast growth of distributed generation capacity, such as PV units in Australia, raises a need for ADNs models to be used by transmission system operators in their dynamic simulations. The maintenance of a combined transmission and distribution systems model being totally impractical, dynamic equivalents are needed.

In this paper, a methodology to identify ADN equivalents has been demonstrated on an real Australian distribution grid hosting SGs and PV units, assumed to follow future grid code.

First, MC simulations are used to account for the uncertainty affecting the unreduced ADN model. Then, a weighted least-square minimization problem is solved to make the response of the equivalent approach the average of the randomized responses where the weights reflect the dispersion of the dynamic responses. Moreover, multiple disturbances are considered and a procedure is used to involve the smallest possible sub-set of them in the least-square minimization, with a guarantee of accuracy with respect to non-trained scenarios. Finally, a method is used to discard from the minimization those parameters with less significant impact.

Simulation results show that the equivalent can reproduce the discontinuous controls of PV units, in particular the disconnection of some of them under low voltage conditions. Accuracy has been also checked in response to disturbances not used for training.

An extension of this research is to consider a situation without retro-fitting of existing PV units. It is expected that this will increase the fraction of these IBGs that disconnect during the disturbances. However, the methodology outlined in this paper would still apply. Indeed, one advantage of grey-box models is their ability to reflect changes in IBG control characteristics.

Appendix. Network reduction

Let us denote by $\underline{\boldsymbol{Y}}_{\boldsymbol{net}}$ the nodal admittance matrix of the unreduced network, as shown in Fig. 2, but without the main transformer. The procedure hereafter aims at finding a reference value for the equivalent impedances, namely $R_a + jX_a$ for the equivalent load, $R_b + jX_b$ for the equivalent IBG and $R_c + jX_c$ for the equivalent SG, see Fig. 8. The derivation focuses on $R_a + jX_a$ but a similar procedure applies to the other two impedances.

First, the load connected to a bus i is replaced by an admittance consuming the same complex power:

$$Y_{ld}(i) = \frac{P(i) - jQ(i)}{|\bar{V}(i)|^2} \tag{9}$$

where $P(i)$ and $Q(i)$ are the active and reactive power consumed by the load at bus i and $|\bar{V}(i)|$ is the magnitude of the voltage at bus i. The nodal admittance matrix $\underline{\boldsymbol{Y}}$ of the combined network and loads is obtained by adding the Y_{ld} values to the corresponding diagonal terms of $\underline{\boldsymbol{Y}}_{\boldsymbol{net}}$, i.e.

$$\begin{aligned} \underline{\boldsymbol{Y}}(i,j) &= \underline{\boldsymbol{Y}}_{\boldsymbol{net}}(i,j) \qquad for\ i \neq j \\ \underline{\boldsymbol{Y}}(i,i) &= \underline{\boldsymbol{Y}}_{\boldsymbol{net}}(i,i) + Y_{ld}(i). \end{aligned} \tag{10}$$

The equivalent impedance seen from the entry point of the network (bus 2 in Fig. 2) is given by the corresponding diagonal term $\underline{\boldsymbol{Z}}(2,2)$ of the impedance matrix:

$$\underline{\boldsymbol{Z}} = \underline{\boldsymbol{Y}}^{-1}. \tag{11}$$

As shown in Fig. 19, $\underline{\boldsymbol{Z}}(2,2)$ is also the sought impedance $R_a + jX_a$ in series with a lumped impedance representing all loads in parallel, i.e.

$$\frac{1}{Y_{ldtot}} = \frac{1}{\sum_i Y_{ld}(i)} \ . \tag{12}$$

The $R_a + jX_a$ impedance is thus simply obtained as:

$$R_a + jX_a = \underline{\boldsymbol{Z}}(2,2) - \frac{1}{Y_{ldtot}} \ . \tag{13}$$

This technique has been found to provide a good initial estimate of the network equivalent impedances. Indeed, none of them is retained in the identification after applying the procedure of Section 4.4.

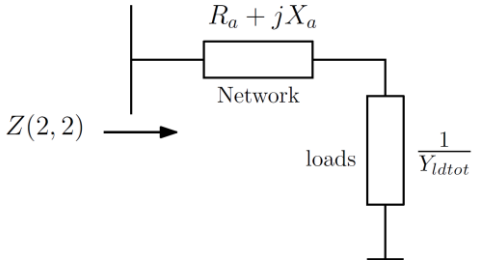

Figure 19 Network reduction technique to estimate the equivalent impedance $R_a + jX_a$

References

[1] S.M Zali and J. Milanovic, "Generic Model of Active Distribution Network for Large Power System Stability Studies," *IEEE trans. on Power Systems,* vol. 28, no. 3, pp. 3126-3133, 2013.

[2] Australian Energy Market Operator (AEMO) , "Response of existing PV inverters to frequency disturbances," AEMO Information & Support Hub, Australia, 2016.

[3] M. G. Dozein, P. Mancarella, T. K. Saha and R. Yan, "System Strength and Weak Grids: Fundamentals, Challenges and Mitigation Strategies," *2018 Australasian Universities Power Engineering Conference (AUPEC),* pp. 1-7, Auckland, New Zealand, 2018.

[4] Australian Energy Market Operator (AEMO) , "reactive po," April 2019.

[5] C. W. Taylor, *Power System Voltage Stability.* Mc Graw Hill, EPRI Power Engineering Series, 1994.

[6] IEEE Standards Coordinating Committee 21, "IEEE Standard Interconnection and Interoperability of Distributed Energy Resources with Associated Electric Power Systems Interfaces," Approved 15 February, 2018.

[7] Commission Regulation (EU) 2016/631 of 14 April 2016 establishing a network code requirements for grid connection of generators," pp. 1-68, 27 April 2016. Available: https://www.entsoe.eu/network_codes/rfg/ [Accessed October 2019].

[8] C. Robert and G. Casella, *Monte-Carlo Statistical Methods.* Springer Science & Business Media, 2013.

[9] G. Chaspierre, P. Panciatici and T. Van Cutsem, "Modelling Active Distribution Networks under Uncertainty: Extracting Parameter Sets from Randomized Dynamic Responses," *Proc. 20th PSCC conference,* Dublin (Ireland), 2018.

[10] J. Milanovic (Convener), "Modelling and aggregation of loads in flexible power networks," *Report of CIGRE WG C4.605,* 2014.

[11] N. Hatziargyriou (Convener), "Contribution to Bulk System Control and Stability by Distributed Energy Resources connected at Distribution Network," *IEEE PES Tech. Report PES-TR22,* 2017.

[12] G. Chaspierre, G. Denis, P. Panciatici and T. Van Cutsem, "Dynamic equivalent of an active distribution network taking into account model uncertainties," *Proc. 13th IEEE PES PowerTech conf.,* Milan (Italy), 2019.

[13] B. Weise, "Impact of k-factor and active current reduction during fault-ride-through of generating units connected via voltage-sourced converters on power system stability," *IET Renewable Power Generation,* vol. 9, no. 1, pp. 25-36, 2015.

[14] G. Chaspierre, P. Panciatici and T. Van Cutsem, "Dynamic Equivalent of a Distribution Grid Hosting Dispersed Photovoltaic Units," *Proc. IREP'17 Symposium,* Espinho (Portugal), 2017.

[15] P. Kundur, *Power System Stability and Control.* McGraw hill New York, 1994.

[16] IEEE Power Engineering Society, "IEEE Recommended Practice for Excitation System Models for Power System Stability Studies," *Technical report,* 2005.

[17] North American Electric Reliability Corporation (NERC), "Distributed Energy Resources Connection Modeling and Reliability Considerations," February 2017.

[18] P. Pourbeik, J. Weber, D. Ramasubramanian, J. Sanchez-Gasca, J. Senthil, P. Zadkhast, J. C. Boemer, A. Gaikwad, I. Green, S. Tacke, R. Favela, S. Wang, S. Zhu and M. Torgesen, "An aggregated dynamic model for distributed energy resources for power system stability studies," *Cigre Science & Engineering,* no. 14, pp. 38-48, June 2019.

[19] K. V. Price, R. M. Storn and J. A. Lampinen, *Differential Evolution – A practical Approach to Global Optimization,* Springer, 2005.

[20] P. Aristidou, D. Fabozzi, and T. Van Cutsem, "Dynamic Simulation of Large-Scale Power Systems Using a Parallel Schur-Complement-Based Decomposition Method," *IEEE Transactions on Parallel and Distributed Systems,* vol. 25, no. 10, pp. 2561–2570, 2014

Gilles Chaspierre received his M.Sc. degree in Electrical Engineering from University of Liège, Belgium, in 2016. He is currently pursuing a PhD at the same University. His main scientific interests are dynamic modelling of inverter-based generators and identification of active distribution networks equivalents for power system dynamics and stability studies.

Mehdi Ghazavi Dozein Mehdi Ghazavi Dozein is currently a PhD student at the University of Melbourne. He earned his master's degree from The University of Tehran, Iran in 2014. His research interest is power system stability and dynamics with high share of converter-based resources. Also, he is highly interested in the application of power-electronic converters to non-synchronous generations.

Guillaume Denis holds an engineering degree from MINES ParisTech, and a M.S. in Energy Physics from ENS Paris-Saclay France. He received a PhD in Electrical Eng. in 2017. Since, he has joined the R&D department of RTE, the French TSO, to study power system dynamics with up to 100 % power electronic based generation.

Patrick Panciatici graduated from Ecole Supérieure d'Electricité (Supelec), France. He joined EDF R&D in 1985, and RTE in 2003, where he is scientific advisor in the R&D direction. He coordinates and supervises long-term research activities, in particular large projects supported by EU (PEGASE, Twenties, iTesla, e-HIGHWAY2050, Migrate, etc.). He is a member of CIGRE and Fellow member of IEEE and SEE (France). He is the representative of RTE in PSERC (Power Systems Engineering Research Center), USA.

Thierry Van Cutsem graduated in Electrical-Mechanical Engineering from the University of Liège, Belgium, where he obtained the Ph.D. degree and he is now adjunct professor. Since 1980, he has been with the Fund for Scientific Research (FNRS), of which he is now a Research Director. His research interests are in power system dynamics, stability, security, monitoring, control and simulation. He has been active in several CIGRE and IEEE Working Groups. He is a Fellow of the IEEE and SEE (France).